

## Original Research

# In Vivo Magnetic Resonance Elastography of Human Brain at 7 T and 1.5 T

Uwe Hamhaber, PhD,<sup>1\*</sup> Dieter Klatt, PhD,<sup>2</sup> Sebastian Papazoglou, PhD,<sup>2</sup> Maurice Hollmann, PhD,<sup>3</sup> Jörg Stadler, PhD,<sup>4</sup> Ingolf Sack, PhD,<sup>2</sup> Johannes Bernarding, MD, PhD,<sup>3</sup> and Jürgen Braun, PhD<sup>1</sup>

**Purpose:** To investigate the feasibility of quantitative in vivo ultrahigh field magnetic resonance elastography (MRE) of the human brain in a broad range of low-frequency mechanical vibrations.

**Materials and Methods:** Mechanical vibrations were coupled into the brain of a healthy volunteer using a coil-driven actuator that either oscillated harmonically at single frequencies between 25 and 62.5 Hz or performed a superimposed motion consisting of multiple harmonics. Using a motion sensitive single-shot spin-echo echo planar imaging sequence shear wave displacements in the brain were measured at 1.5 and 7 T in whole-body MR scanners. Spatially averaged complex shear moduli were calculated applying Helmholtz inversion.

**Results:** Viscoelastic properties of brain tissue could be reliably determined in vivo at 1.5 and 7 T using both single-frequency and multifrequency wave excitation. The deduced dispersion of the complex modulus was consistent within different experimental settings of this study for the measured frequency range and agreed well with literature data.

**Conclusion:** MRE of the human brain is feasible at 7 T. Superposition of multiple harmonics yields consistent results as compared to standard single-frequency based MRE. As such, MRE is a system-independent modality for measuring the complex shear modulus of in vivo human brain in a wide dynamic range.

**Key Words:** magnetic resonance imaging; brain; elastography; ultra high field; motion encoding; viscoelasticity

**J. Magn. Reson. Imaging 2010;32:577–583.**

© 2010 Wiley-Liss, Inc.

MANY DISEASES are associated with changes in the mechanical properties of body tissue. For this reason palpation is one of the simplest and oldest yet very effective diagnostic methods for soft tissue assessment near the body surface. Elastography based on ultrasound (1,2) or magnetic resonance (3,4) extends our sensation of soft tissue stiffness from the subjective impression of the palpating physician to an objective quantitative measurement as well as beyond the surface into regions of the body which are either difficult to palpate or even traditionally not palpable (5–11). For example, the quantification of brain elasticity has become accessible in vivo through recent developments in magnetic resonance elastography (MRE) without opening the skull by surgical intervention (12–20). Thus, MRE opens the door for a noninvasive measurement of the mechanical structure of the brain in its physiological environment. Micromechanical properties of hierarchic systems are known to scale to global viscoelastic properties given by the dispersion of the complex modulus of a material (21). In recent studies of cerebral MRE the dispersion of the complex modulus of the brain was found to be sensitive to age-related changes of the mechanical matrix of the brain (22) as well as to tissue degradation due to multiple sclerosis (23). In the near future, cerebral MRE might assist neurosurgeons in operation planning, might help biomechanics to clarify brain damage mechanisms occurring at head impact, and might serve as a new quantitative MRI modality for an early detection of neurodegenerative diseases.

Currently, whole-body MRI including imaging of the human brain is proceeding toward ultrahigh magnetic fields at 7 T in order to profit from enhanced MR signal to improve either the signal-to-noise ratio (SNR) or the spatial resolution (24). MRI at 7 T still poses a challenge because of increased B<sub>1</sub>-field inhomogeneity, stronger susceptibility artifacts and changed relaxation times, primarily shortened T<sub>2</sub>. To date the utilization of 7 T magnetic fields in MRE was only preliminarily tested (25) and there exists no analysis of MRE-related quantitative viscoelastic parameters based on data acquired at different magnetic field strengths. The prediction of the results of MRE at different field strengths is not trivial since MRE requires

<sup>1</sup>Institute of Medical Informatics, Charité – Universitätsmedizin Berlin, Berlin, Germany.

<sup>2</sup>Department of Radiology, Charité – Universitätsmedizin Berlin, Berlin, Germany.

<sup>3</sup>Institute of Biometry and Medical Informatics, Otto-von-Guericke University, Magdeburg, Germany.

<sup>4</sup>Leibniz Institute for Neurobiology, Magdeburg, Germany.

Contract grant sponsor: Deutsche Forschungsgemeinschaft; Contract grant number: BR 2235/2.

\*Address reprint requests to: U.H., BioCer Entwicklungs-GmbH, Ludwig-Thoma-Str. 36 c, D-95447 Bayreuth, Germany.  
E-mail: uwe.hamhaber@biocer-gmbh.de

Received November 22, 2009; Accepted June 7, 2010.

DOI 10.1002/jmri.22294

View this article online at [wileyonlinelibrary.com](http://wileyonlinelibrary.com).

a well-balanced adjustment of MRI-related parameters and the mechanical setting of the experiment. For example, the measurement of modulus dispersion at 1.5 T has until recently been based on a superposition of multiple mechanical excitation frequencies (16,26). The encoding of multifrequency vibrations in the brain of up to 62.5 Hz was achieved using four periods of a 60-Hz-sinusoidal motion encoding gradient (MEG) with a total length of 66.7 msec. During that time enhanced signal relaxation at 7 T might affect the quality of wave images in terms of reduced SNR, which in turn might render wave inversion less reliable since the presence of noise yields an underestimation of elastic moduli, particularly at low wave numbers (27). However, the inherently improved SNR at 7 T may counteract this effect and therefore may still enable or potentially improve the analysis of wavelengths by algebraic inversion. Along with this, increased physiological noise at 7 T, causing a biased display of morphological structures (28), may also have an impact on wave patterns and therewith on the outcome of MRE. This complex interaction of mechanical and imaging-related parameters raises the question whether MRE at 7 T yields comparable results to established MRE at lower fields where several comparative studies between MRE and static as well as dynamic mechanical tests showed good quantitative correlations (29–31).

Thus, the aim of the present study was to investigate whether in vivo MRE of the human brain at 7 T is feasible and whether complex shear moduli measured in a broad range of low-frequency mechanical vibrations at 7 T are in agreement with measurements at 1.5 T.

## THEORY

In the following a brief review of the basic theoretical concepts of elasticity MR imaging by planar harmonic shear waves in steady-state is given.

### Phase Encoding

We account for a sinusoidally vibrating isochromat with displacement amplitude  $|\mathbf{u}_0|$ , angular drive frequency  $\omega_u$  and phase offset  $\alpha_u$ . The motion shall be encoded by oscillating gradients  $\mathbf{G}(t)$  with zero momentum for rendering phase encoding independent of isochromat initial position. For a sinusoidal MEG with amplitude  $|\mathbf{G}_0|$ , angular frequency  $\omega_g$ , phase offset  $\alpha_g = 0$  and duration  $\tau = N \frac{2\pi}{\omega_g}$  with integer  $N$ , the accumulated spin phase reads:

$$\phi(\tau) = \pi \gamma \mathbf{G}_0 \mathbf{u}_0 \frac{N}{\omega} \cos(\alpha_u) \quad \text{for} \quad \omega = \omega_g = \omega_u \quad [1]$$

and

$$\phi(\tau) = 2\gamma \mathbf{G}_0 \mathbf{u}_0 \frac{\omega_g}{\omega_u^2 - \omega_g^2} \sin\left(N\pi \frac{\omega_u}{\omega_g}\right) \cos\left(N \frac{\omega_u}{\omega_g} + \alpha_u\right) \quad \text{for} \quad \omega_g \neq \omega_u \quad [2]$$

according to (32,33).  $\alpha_u$  corresponds to the relative phase of the isochromat vibration at the onset of

motion encoding  $\Delta T \omega_u \pmod{2\pi}$ , with  $\Delta T$  being the delay between the onsets of vibration and motion encoding.

### Helmholtz Inversion

The derivation of the Helmholtz inversion is based on the linearized Cauchy equation of motion for small displacements  $\mathbf{u}$  at position  $\mathbf{x}$  and time  $t$  which reads:

$$\nabla \cdot \boldsymbol{\sigma}(\mathbf{x}, t) + \mathbf{b}(\mathbf{x}, t) = \rho(\mathbf{x}, t) \ddot{\mathbf{u}}(\mathbf{x}, t), \quad [3]$$

with  $\boldsymbol{\sigma}$  being the Cauchy stress tensor,  $\mathbf{b}$  the body-force vector, and  $\rho$  the material's density. Dots above symbols refer to the order of differentiation with respect to time.

We now assume a homogeneous, isotropic, linear viscoelastic material behavior:

$$\boldsymbol{\sigma}(\mathbf{x}, t) = \psi_\lambda(t) * \text{tr}(\dot{\boldsymbol{\epsilon}}(\mathbf{x}, t)) \mathbf{I} + 2\psi_G(t) * \dot{\boldsymbol{\epsilon}}(\mathbf{x}, t), \quad [4]$$

wherein  $\psi_\lambda$  and  $\psi_G$  are relaxation functions of the Heavyside type corresponding to the first and second Lamé constants of the linear elastic case (34).  $f * g$  delineates the temporal convolution of functions  $f$  and  $g$ , and  $\text{tr}()$  indicates the trace of a second order tensor.  $\mathbf{I}$  is the second order identity tensor and  $\dot{\boldsymbol{\epsilon}}$  is the strain rate tensor, which for small displacements becomes linear:

$$\dot{\boldsymbol{\epsilon}}(\mathbf{x}, t) = \frac{1}{2} \left( \nabla \dot{\mathbf{u}}(\mathbf{x}, t) + (\nabla \dot{\mathbf{u}}(\mathbf{x}, t))^T \right). \quad [5]$$

Therewith, in absence of body forces for a material with homogeneous and stationary density equation [3] results in the Navier equation:

$$\begin{aligned} (\dot{\psi}_\lambda(t) + \dot{\psi}_G(t)) * \nabla(\nabla \cdot \mathbf{u}(\mathbf{x}, t)) + \dot{\psi}_G(t) * \Delta \mathbf{u}(\mathbf{x}, t) \\ = \rho \ddot{\mathbf{u}}(\mathbf{x}, t). \end{aligned} \quad [6]$$

Here,  $\Delta$  is the Laplace operator.

Using the decomposition  $\mathbf{u} = \mathbf{u}_s + \mathbf{u}_p$  with  $\nabla \cdot \mathbf{u}_s = 0$  and  $\nabla \times \mathbf{u}_p = \mathbf{0}$ , Eq. [6] can be separated into two independent wave equations that are valid for shear and pressure waves, respectively. The wave equation for shear waves is given by:

$$\dot{\psi}_G(t) * \Delta \mathbf{u}_s(\mathbf{x}, t) = \rho \ddot{\mathbf{u}}_s(\mathbf{x}, t). \quad [7]$$

As the components of the vector equation [7] are decoupled, any arbitrary aligned component  $u_s$  of a shear displacement vector field  $\mathbf{u}_s$  provides the same material parameters. Considering only one such component, Eq. [7] reduces to the scalar shear wave equation:

$$\dot{\psi}_G(t) * \Delta u_s(\mathbf{x}, t) = \rho \ddot{u}_s(\mathbf{x}, t). \quad [8]$$

For continuous and piecewise smooth functions  $u_s(\mathbf{x}, t)$  that fulfil  $u_s(\mathbf{x}, t) \in L^1$  and  $\dot{u}_s(\mathbf{x}, t) \in L^1$  in the time domain, the temporal Fourier-transform of the scalar wave Equation [8] leads to the scalar Helmholtz equation for shear waves in the frequency domain:

$$G^*(\omega) \Delta U_s(\mathbf{x}, \omega) = -\rho \omega^2 U_s(\mathbf{x}, \omega). \quad [9]$$

The complex shear modulus  $G^*(\omega)$  is the Fourier transform of  $\dot{\psi}_G(t)$ , and  $U_S(\mathbf{x}, \omega)$  is the scalar shear displacement in the frequency domain. In materials science the real and imaginary parts of the complex shear modulus are denoted as shear storage modulus  $G'$  and shear loss modulus  $G''$ . In Eq. [9] the complex shear modulus is spatially independent due to the material's homogeneity assumption and therefore this equation is in a strict sense not valid for heterogeneous material. However, the additional assumption of a locally homogeneous medium allows the complex shear modulus to be determined for each local region  $R_i$  separately. Thus, in case of a planar shear wave propagating within the xy-plane, Eq. [9] rearranged for the complex shear modulus reduces to:

$$G^*(R_i, \omega) = -\rho\omega^2 \frac{U_S(x, y, \omega)}{\frac{\partial^2}{\partial x^2} U_S(x, y, \omega) + \frac{\partial^2}{\partial y^2} U_S(x, y, \omega)} \quad \text{for } (x, y) \in R_i \quad [10]$$

according to (9), which is a special case of the inversions presented in (35) and (36).

## MATERIALS AND METHODS

Experiments were performed on a healthy male volunteer after giving written consent according to the local boards of ethics and the Declaration of Helsinki. Measurements were performed on a 1.5 T whole-body MR scanner (Magnetom Sonata, Siemens, Erlangen, Germany) using a standard head coil as well as on a 7 T whole-body MR scanner (Siemens) using an 8-channel phased-array TX/TR head coil operating in single-channel mode during TX. The gradient systems allowed a maximum gradient amplitude of 40 mT/m at 1.5 T and 32 mT/m at 7 T as well as a maximum slew rate of 200 mT/(m · s) and 170 mT/(m · s) for the 1.5 T and 7 T scanners. For better comparison, experimental settings such as driver, image resolution, and the method of wave analysis were kept identical for both field strengths in all experiments.

### Wave Excitation and Image Acquisition

A coil-driven custom-built bite bar (14) was used to introduce shear waves into the brain of the volunteer (Fig. 1) at four drive frequencies  $f_u = \omega_u/(2\pi) = 25.0, 37.5, 50.0,$  and  $62.5$  Hz in four consecutive single-frequency experiments. Furthermore, multifrequency MRE was performed utilizing a superposition of all four drive frequencies with equal amplitudes.

Nonferromagnetic materials (aluminum coil sockets, copper wire, polymer screws, and a carbon fiber reinforced polymer bar) were used for the construction of the actuator bite bar. For a good transmission of vibrations, a form fit was achieved using flasking plaster. The bite bar was fixed by a moderate biting force of the volunteer during MRE experiments.

All experiments were run both at 1.5 T and 7 T using a single-shot spin-echo echo planar imaging (EPI) sequence modified to capture displacement wave images inside the brain by encoding motions perpen-

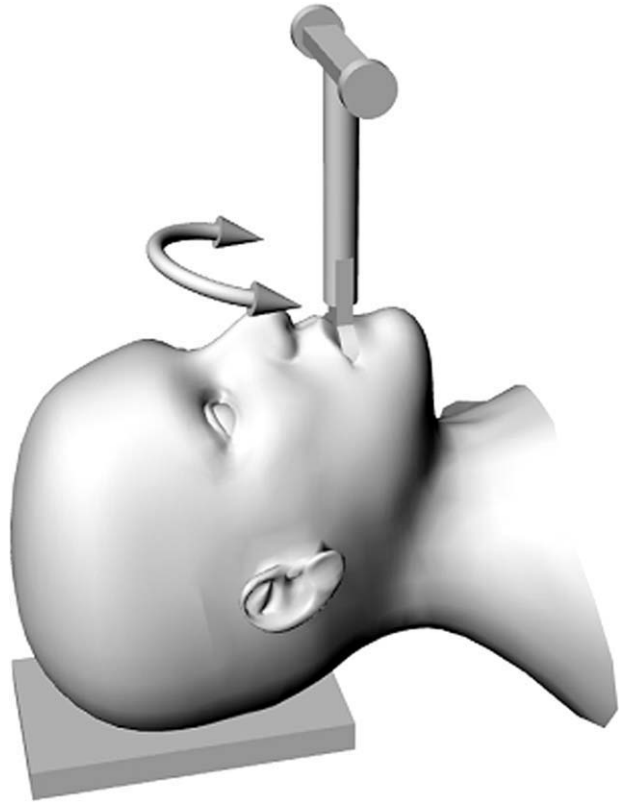


**Figure 1.** Excitation device and resulting head motion (arrow). A superposition of a slight nodding and a left-to-right motion is assumed due to the complex bearing of the head on the neck and examination table.

dicular to the image plane (14). Motion encoding for the single-frequency experiments was achieved by using single cycle sinusoidal MEGs of matched frequencies  $f_g = \omega_g/(2\pi) = f_u$  which were inserted between the  $90^\circ$  and  $180^\circ$  radiofrequency (RF) pulses. For multifrequency experiments broadband motion encoding was achieved by applying a double cycle sinusoidal MEG of  $f_g = 60$  Hz. Axial slices at 5–10 mm above the lateral ventricles were acquired with  $192 \times 192$  mm<sup>2</sup> field of view,  $64 \times 64$  matrix, and 6 mm slice thickness. Repetition time (TR) was kept constant at 3 seconds. For both field strengths echo time (TE) was adjusted to about 96, 69, 64, and 64 msec for 25, 37.5, 50, and 62.5 Hz motion encoding in single frequency MRE, and to about 82 msec in multifrequency MRE. By setting  $\Delta T$ , the time delay between the start of the mechanical vibration and the start of the MEG, in the range of 250 msec to 500 msec for different drive frequencies a steady-state of the shear wave field was achieved before motion encoding was applied. As  $\Delta T$  corresponds to the temporal phase of the mechanical wave,  $\Delta T$  was varied 20 times by a time increment of  $\Delta t = 1/(20f_u)$  for repeated acquisitions of single wave images to acquire the temporal evolution of the displacement wave field during one vibration period in case of single-frequency MRE. For multifrequency MRE a  $\Delta t$  of 2 msec was applied to vary  $\Delta T$  40 times resulting in a time shift of 80 msec which corresponds to 2, 3, 4, and 5 cycles of a 25,

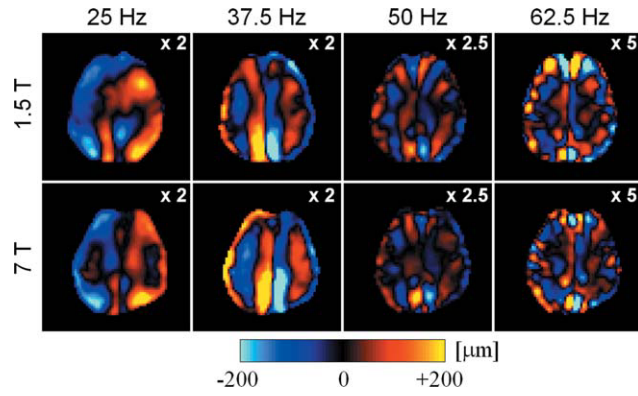


**Figure 2.** Out-of-plane displacement wave images in axial slice position at different drive frequencies acquired by single-frequency MRE. Changes in the wave patterns are due to different excitation frequencies. For the purpose of display the displacements have been multiplied by the factors indicated at the right upper corners.

37.5, 50, and 62.5 Hz vibration, respectively. For each  $\Delta T$  of the resulting temporal image series two wave images were acquired with inverted MEG polarity leading to an acquisition time of 120 seconds and 240 seconds for single-frequency and multifrequency measurement series. All measurement series were repeated three times for the evaluation of reproducibility.

### Data Analysis

Measured phase images were converted into displacement images using Eqs. [1] and [2]. Complex subtraction of displacement images with inverted MEG was accomplished for eliminating static phase shifts. Phase unwrapping was applied for each subtraction image prior to temporal Fourier-transformation of the measured displacement image time series  $u(x_i, y_j, t_k)$ . To suppress noise and pressure wave components the resulting complex wave images  $U(x_i, y_j, \omega_k)$  at drive frequencies  $\omega_k$  were subjected to spatial Butterworth-like filters of lower/upper wavelength thresholds of 1.26/14.75, 1.13/8.44, 1.09/5.83 and 1.07/4.76 cm for  $f_u = 25, 37.5, 50$  and 62.5 Hz, respectively, resulting in approximately pure shear wave images  $U_s(x_i, y_j, \omega_k)$ . Assuming that the neighborhood of each pixel  $(x_i, y_j)$  is a locally homogeneous material region, and that the shear wave propagates within the image plane (set to the  $xy$ -plane), complex shear modulus reconstruction was applied according to Eq. [10] on a pixel-by-pixel basis using the discrete second-order derivative approximation  $\frac{f_{i+2} - 2f_i + f_{i-2}}{4\Delta s^2}$  for  $x$  and  $y$  directions. Furthermore, a homogeneous brain density  $\rho$  of 1000 kg/m<sup>3</sup> was assumed. By taking the median, the complex shear modulus was spatially averaged over the entire parenchyma depicted in the according image slice. Mean values and standard deviations of shear storage and shear loss modulus were calculated for repeated measurements.

## RESULTS

Figures 2 and 3 show series of wave images acquired with single-frequency and multifrequency excitation

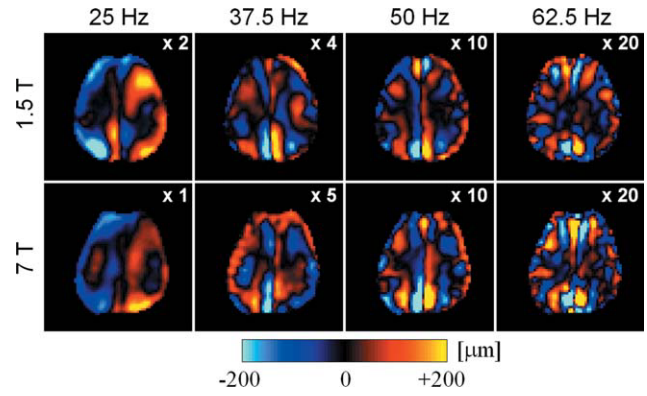


**Figure 3.** Out-of-plane displacement wave images in axial slice position at different drive frequencies acquired by multifrequency MRE. Changes in the wave patterns are due to different excitation frequencies. For the purpose of display the displacements have been multiplied by the factors indicated in the right upper corners.

at 7 T and 1.5 T. All four techniques led to similar wave patterns for corresponding excitation frequencies. As an example, Figs. 4 and 5 depict maps of shear storage modulus ( $G'$ ) and shear loss modulus ( $G''$ ) calculated by Eq. [10] for both field strengths. The spatially resolved maps of storage and loss modulus differ between 7 T and 1.5 T, whereas spatially averaged values show good agreement. Spatially averaged values of shear storage and shear loss modulus of the brain parenchyma are summarized in Table 1.

Considering the different magnetic field strengths and all applied excitation frequencies, storage moduli were found in a range between 1.1 kPa and 2.5 kPa. Shear loss moduli range between 0.4 kPa and 0.8 kPa. A good reproducibility of the data is indicated by small standard deviations of 1% to 3% for the storage moduli and 2% to 8% for the shear loss moduli related to repeated measurements.

For both single-frequency and multifrequency excitation, the storage and loss moduli show similar

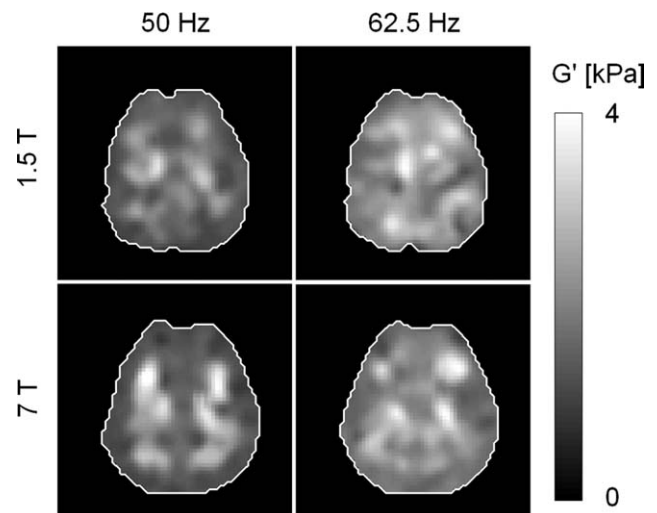


**Figure 4.** Shear storage modulus ( $G'$ ) maps of axial brain slices resulting from single-frequency excitation for frequencies of 50 Hz and 62.5 Hz measured at 7 T and 1.5 T.

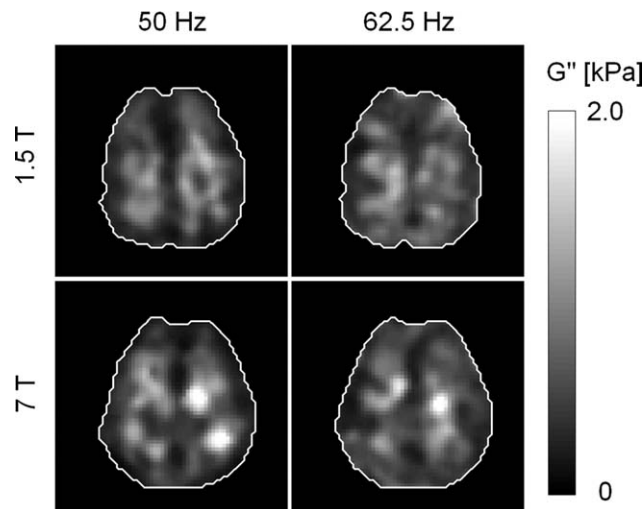


**Figure 5.** Shear loss modulus ( $G''$ ) maps of axial brain slices resulting from single-frequency excitation for frequencies of 50 Hz and 62.5 Hz measured at 7 T and 1.5 T.

frequency dependencies at 1.5 T and 7 T with increasing values for increasing frequencies except for a reduction of the shear loss moduli measured by the single-frequency method at 7 T and 50 Hz.

SNR was analyzed using magnitude images at 1.5 T and 7 T (Table 2). A good correlation was found between increasing SNR and decreasing TE at 1.5 T independent of single- or multifrequency excitation. A similar behavior could be seen for the 7 T data apart from a signal drop in a multifrequent MRE experiment performed at an intermediate TE. Except from this outlier, all SNRs were comparable between 1.5 T and 7 T.

**DISCUSSION**

MRE was successfully implemented at 7 T using a coil-driven bite bar and a motion-sensitive single-shot spin-echo EPI sequence. This proved the feasibility of MRE at 7 T with hardware and MR sequences developed for lower field strengths.

As only nonferromagnetic materials were used for the construction of the actuator bite bar, no interactions with the magnetic field inside the magnet were observed at either field strength. A slight heating of the aluminum coil sockets to about 50°C could only be observed at 1.5 T. This is due to the fact that here

a 4.7-fold electrical current is needed to produce vibration amplitudes comparable to those at 7 T. In addition, potential risks are minimized by the placement of the aluminum coil sockets outside the MR head coil with a safety clearance of 15 cm between the aluminum coil sockets and the head of the volunteer. Thus, coil-driven actuators known for robustness and easy handling remain a good option at 7 T, and even profit from higher field strength.

Analyses of the safety of MRE including studies of the brain were published recently (37,38). The results indicate that the vibrational amplitudes used for mechanical excitation in MRE are below the whole-body vibration limit imposed by the European Union and that based on measurements of heart rate and blood pressure as well as on electroencephalography brain MRE is safe to perform on human subjects. Thus, according to the current state of knowledge in vivo MRE of the human brain can be considered harmless.

The EPI-based sequence allowed short acquisition times. This will help to improve patient comfort by reducing the total time necessary for applying mechanical vibrations. The well-known drawbacks in single-shot EPI such as long effective echo times, local signal reductions, and image distortion (39) had negligible effects on spatially averaged storage and loss moduli. This is supported by the analysis of the SNR in EPI data acquired at 1.5 T and 7 T. Comparable SNR values were observed due to similar sequence echo times at both field strengths. Except for one outlier in a multifrequency MRE experiment at 7 T, the expected increase in SNR with decreasing echo time was found for both field strengths. Overall, the appearance of wave patterns at both 1.5 T and 7 T was very similar. As SNR, spatial intensity variations, and overall image quality intrinsically influence the MRE results minor differences in the parameter maps were expected at 1.5 T and 7 T. Relative deviations of storage moduli between the two field strengths were below 10% in single-frequency MRE and below 20% in multifrequency MRE. The respective deviations of loss moduli were within the margins of 15% and 30%. These discrepancies are within the range of variability of planar MRE encountered in examinations on different days with slightly varying volunteer position and image slice alignment (18). Comparable standard deviations in both field strengths indicate that the potential increase of SNR at 7 T may have been counterbalanced by a decreased  $T_2$  relaxation (40) and a

Table 1  
Spatially Averaged Shear Storage Moduli  $G' = \Re\{G^*\}$  and Shear Loss Moduli  $G'' = \Im\{G^*\}$  Both in Pa With Standard Deviation ( $\pm$ SD) of Repeated Measurements

$f_u$	Single-frequency MRE				Multifrequency MRE			
	1.5 T		7 T		1.5 T		7 T	
	$G'$	$G''$	$G'$	$G''$	$G'$	$G''$	$G'$	$G''$
25.0	1170 $\pm$ 17	493 $\pm$ 38	1252 $\pm$ 15	543 $\pm$ 9	1055 $\pm$ 22	433 $\pm$ 12	1250 $\pm$ 23	578 $\pm$ 18
37.5	1574 $\pm$ 31	536 $\pm$ 10	1504 $\pm$ 33	551 $\pm$ 13	1596 $\pm$ 36	538 $\pm$ 19	1743 $\pm$ 22	644 $\pm$ 34
50.0	1897 $\pm$ 34	583 $\pm$ 15	1811 $\pm$ 27	532 $\pm$ 12	1965 $\pm$ 27	612 $\pm$ 16	2047 $\pm$ 39	677 $\pm$ 43
62.5	2482 $\pm$ 82	707 $\pm$ 16	2211 $\pm$ 23	608 $\pm$ 11	2540 $\pm$ 49	765 $\pm$ 35	2546 $\pm$ 23	729 $\pm$ 17

Values are given depending on excitation mode (single-frequency and multifrequency), excitation frequency ( $f_u$  in Hz) and field strength.

Table 2  
Mean Signal-to-Noise Ratio (m-SNR) as a Function of Echo Time (TE in msec) and Excitation Frequency ( $f_u$  in Hz) in Single-Frequency and Multifrequency Experiments at 1.5 T and 7 T

$f_u$	1.5 T		7 T	
	m-SNR	TE	m-SNR	TE
Single-frequency MRE				
25.0	35.5 ± 2.4	95.54	33.0 ± 2.4	95.96
37.5	49.2 ± 3.3	68.86	49.9 ± 6.8	69.28
50.0	50.7 ± 4.3	64.28	58.6 ± 4.1	63.62
62.5	51.3 ± 3.4	64.28	56.4 ± 1.4	63.62
Multifrequency MRE				
	40.3 ± 0.2	82.18	29.9 ± 1.7	82.60

Mean values and standard deviations ( $\pm$ SD) were calculated from four repeated individual MRE experiments. SNR values for individual MRE experiments were determined by spatially averaging the signal in a quadratic 8x8 region of interest in the brain tissue as well as in the background and taking the ratio of these averaged signals.

more pronounced spatial variation of  $T_2^*$  due to increased susceptibility artifacts as well as increased physiologic noise. Spatial variations in the modulus maps can be mitigated by accounting for “global” viscoelastic parameters. The spatially averaged values determined in this study are in good agreement with in vivo MRE data reported by other groups (13,16,18–20).

Improvements in wave image quality at 7 T are expected when accounting for the faster signal decay of brain tissue at high field strengths due to shortened  $T_2$  times. Therefore, shorter echo times are required for high-field MRE. In in vivo MRE with low frequency vibrations TE is mainly determined by the duration of the MEG and cannot be reduced further by shortening readout methods such as parallel or segmented imaging. In future studies a shorter MEG of one or two periods of 60 Hz center frequency might be used for encoding oscillations from 25 Hz to 62.5 Hz. It remains to be determined whether the resulting low encoding fraction (41) yields sufficiently high phase signals for in vivo brain oscillations. Besides these considerations, parallel imaging would certainly improve the image quality by reducing physiological noise and decreasing  $B_1$ -field inhomogeneities (42). Optimization of single-shot EPI for the application at 7 T is an ongoing issue including topics such as automatic correction of geometric distortions as well as reduction of signal dropouts, specific absorption rate, and acoustic noise (43).

In conclusion, it was shown that MRE is feasible at 7 T, and that the results are comparable to those achieved at 1.5 T using the same drivers, MRE sequences, and processing software at both field strengths. It was demonstrated that within the dynamic range between 25 Hz and 62.5 Hz both single-frequency and multifrequency MRE yield consistent results. This promising finding encourages the optimization of both MRI scanner hardware and software for the needs at 7 T to fully exploit the potential of ultrahigh field MRE. It is to be expected that enhanced SNR will ameliorate considerably the quality of wave images and will allow a more precise determination of spatial parameter maps of viscoelasticity.

## REFERENCES

- Parker KJ, Huang SR, Musulin RA, Lerner RM. Tissue response to mechanical vibrations for “sonoelasticity imaging”. *Ultrasound Med Biol* 1990;16:241–246.
- Ophir J, Céspedes I, Ponnekanti H, Yazdi Y, Li X. Elastography: a quantitative method for imaging the elasticity of biological tissues. *Ultrasound Imaging* 1991;13:111–134.
- Muthupillai R, Lomas DJ, Rossman PJ, Greenleaf JF, Manduca A, Ehman RL. Magnetic resonance elastography by direct visualization of propagating acoustic strain waves. *Science* 1995;269:1854–1857.
- Plewes DB, Betty I, Urchuk SN, Soutar I. Visualizing tissue compliance with MR imaging. *J Magn Reson Imaging* 1995;5:733–738.
- Sandrin L, Fourquet B, Hasquenoph JM, et al. Transient elastography: a new noninvasive method for assessment of hepatic fibrosis. *Ultrasound Med Biol* 2003;29:1705–1713.
- Kemper J, Sinkus R, Lorenzen J, Nolte-Ernsting C, Stork A, Adam G. MR elastography of the prostate: initial in-vivo application. *Rofo* 2004;176:1094–1099.
- Rouviere O, Yin M, Dresner MA, et al. MR elastography of the liver: preliminary results. *Radiology* 2006;240:440–448.
- Huwart L, Peeters F, Sinkus R, et al. Liver fibrosis: non-invasive assessment with MR elastography. *NMR Biomed* 2006;19:173–179.
- Klatt D, Asbach P, Rump J, et al. In vivo determination of hepatic stiffness using steady-state free precession magnetic resonance elastography. *Investig Radiol* 2006;41:841–848.
- Sinkus R, Tanter M, Xydeas T, Catheline S, Bercoff J, Fink M. Viscoelastic shear properties of in vivo breast lesions measured by MR elastography. *Magn Reson Imaging* 2005;23:159–165.
- Elgeti T, Rump J, Papazoglou S, et al. Cardiac magnetic resonance elastography — initial results. *Investig Radiol* 2008;43:762–772.
- Manduca A, Lake DS, Kruse SA, Ehman RL. Spatio-temporal directional filtering for improved inversion of MR elastography images. *Med Image Anal* 2003;7:465–473.
- McCracken PJ, Manduca A, Felmlee J, Ehman RL. Mechanical transient-based magnetic resonance elastography. *Magn Reson Med* 2005;53:628–639.
- Hamhaber U, Sack I, Papazoglou S, Rump J, Klatt D, Braun J. Three-dimensional analysis of shear wave propagation observed by in vivo magnetic resonance elastography of the brain. *Acta Biomater* 2007;3:127–137.
- Xu L, Lin Y, Han JC, Xi ZN, Shen H, Gao PY. Magnetic resonance elastography of brain tumors: preliminary results. *Acta Radiol* 2007;48:327–330.
- Klatt D, Hamhaber U, Asbach P, Braun J, Sack I. Noninvasive assessment of the rheological behavior of human organs using multifrequency MR elastography: a study of brain and liver viscoelasticity. *Phys Med Biol* 2007;52:7281–7294.
- Xu L, Lin Y, Xi ZN, Shen H, Gao PY. Magnetic resonance elastography of the human brain: a preliminary study. *Acta Radiol* 2007;48:112–115.
- Sack I, Beierbach B, Hamhaber U, Klatt D, Braun J. Non-invasive measurement of brain viscoelasticity using magnetic resonance elastography. *NMR Biomed* 2008;21:265–271.
- Kruse SA, Rose GH, Glaser KJ, et al. Magnetic resonance elastography of the brain. *Neuroimage* 2008;39:231–237.
- Green MA, Bilston LE, Sinkus R. In vivo brain viscoelastic properties measured by magnetic resonance elastography. *NMR Biomed* 2008;21:755–764.
- Verdier C. Rheological properties of living materials. From cell to tissues. *J Theor Med* 2003;5:67–91.
- Sack I, Beierbach B, Wuerfel J, et al. The impact of aging and gender on brain viscoelasticity. *Neuroimage* 2009;46:265–271.
- Wuerfel J, Paul F, Beierbach B, et al. MR-elastography reveals degradation of tissue integrity in multiple sclerosis. *Neuroimage* 2010;49:2520–2525.
- Hu XP, Norris DG. Advances in high-field magnetic resonance imaging. *Annu Rev Biomed Eng* 2004;6:157–184.
- Maderwald S, Kraff O, de Greiff A, et al. In vivo and in vitro 7T MR elastography with parallel imaging. In: *Proc 15th Annual Meeting ISMRM, Berlin; 2007 (abstract 1254)*.
- Asbach P, Klatt D, Hamhaber U, et al. Assessment of liver viscoelasticity using multifrequency MR elastography. *Magn Reson Med* 2008;60:373–379.
- Papazoglou S, Hamhaber U, Braun J, Sack I. Algebraic Helmholtz inversion in planar magnetic resonance elastography. *Phys Med Biol* 2008;53:3147–3158.

28. Bianciardi M, Fukunaga M, van Gelderen P, et al. Sources of functional magnetic resonance imaging signal fluctuations in the human brain at rest: a 7 T study. *Magn Reson Imaging* 2009;27:1019–1029.
29. Hamhaber U, Grieshaber FA, Nagel JH, Klose U. Comparison of quantitative shear wave MR-elastography with mechanical compression tests. *Magn Reson Med* 2003;49:71–77.
30. Ringleb SI, Chen Q, Lake DS, Manduca A, Ehman RL, An KN. Quantitative shear wave magnetic resonance elastography: comparison to a dynamic shear material test. *Magn Reson Med* 2005;53:1197–1201.
31. Vappou J, Breton E, Choquet P, Goetz C, Willinger R, Constantinesco A. Magnetic resonance elastography compared with rotational rheometry for in vitro brain tissue viscoelasticity measurement. *Magn Reson Mater Phys Biol Med* 2007;20:273–278.
32. Muthupillai R, Rossman PJ, Lomas DJ, Greanleaf JF, Riederer SJ, Ehman RL. Magnetic resonance imaging of transverse acoustic strain waves. *Magn Reson Med* 1996;36:266–274.
33. Sack I, McGowan CK, Samani A, Luginbuhl C, Oakden W, Plewes DB. Observation of nonlinear shear wave propagation using magnetic resonance elastography. *Magn Reson Med* 2004;52:842–850.
34. Carcione JM. Wave fields in real media: wave propagation in anisotropic, anelastic, porous and electromagnetic media. Amsterdam: Elsevier; 2007.
35. Oliphant TE, Manduca A, Ehman RL, Greenleaf JF. Complex-valued stiffness reconstruction for magnetic resonance elastography by algebraic inversion of the differential equation. *Magn Reson Med* 2001;45:299–310.
36. Sinkus R, Tanter M, Catheline S, et al. Imaging anisotropic and viscous properties of breast tissue by magnetic resonance-elastography. *Magn Reson Med* 2005;53:372–387.
37. Ehman EC, Rossman PJ, Kruse SA, Sahakian AV, Glaser KJ. Vibration safety limits for magnetic resonance elastography. *Phys Med Biol* 2008;53:925–935.
38. Liu GR, Gao PY, Lin Y, et al. Brain magnetic resonance elastography on healthy volunteers: a safety study. *Acta Radiol* 2009;50:423–429.
39. Schmitt F, Stehling MK, Turner R. Echo-planar imaging: theory, technique and application. Berlin: Springer; 1998.
40. Michaeli S, Garwood M, Zhu XH, et al. Proton T2 relaxation study of water, N-acetylaspartate, and creatine in human brain using Hahn and Carr-Purcell spin echoes at 4T and 7T. *Magn Reson Med* 2002;47:629–633.
41. Rump J, Klatt D, Braun J, Warmuth C, Sack I. Fractional encoding of harmonic motions in MR elastography. *Magn Reson Med* 2007;57:388–395.
42. Wiesinger F, Van de Moortele PF, Adriany G, De Zanche N, Ugurbil K, Pruessmann KP. Potential and feasibility of parallel MRI at high field. *NMR Biomed* 2006;19:368–378.
43. Speck O, Stadler J, Zaitsev M. High resolution single-shot EPI at 7T. *Magn Reson Mater Phys Biol Med* 2008;21:73–86.